

NOTE

Intan Technologies integrated circuits can produce analog-to-digital conversion artifacts that affect neural signal acquisition

To cite this article: Katrina Barth *et al* 2024 *J. Neural Eng.* **21** 044001

View the [article online](#) for updates and enhancements.

You may also like

- [Evaluating and benchmarking the EEG signal quality of high-density, dry MXene-based electrode arrays against gelled Ag/AgCl electrodes](#)

Brian Erickson, Ryan Rich, Sneha Shankar et al.

- [Open Ephys: an open-source, plugin-based platform for multichannel electrophysiology](#)

Joshua H Siegle, Aarón Cuevas López, Yogi A Patel et al.

- [NeuroDAC: an open-source arbitrary biosignal waveform generator](#)

M P Powell, J Anso, R Gilron et al.

Journal of Neural Engineering



NOTE

RECEIVED
22 March 2024

REVISED
17 May 2024

ACCEPTED FOR PUBLICATION
12 June 2024

PUBLISHED
9 July 2024

Intan Technologies integrated circuits can produce analog-to-digital conversion artifacts that affect neural signal acquisition

Katrina Barth¹ , Cecilia Schmitz¹ , Thomas Jochum¹ and Jonathan Viventi^{1,2,3,4,5,*}

¹ Department of Biomedical Engineering, Duke University, Durham, NC, United States of America

² Department of Neurobiology, Duke University School of Medicine, Durham, NC, United States of America

³ Department of Neurosurgery, Duke University School of Medicine, Durham, NC, United States of America

⁴ Department of Neurology, Duke University School of Medicine, Durham, NC, United States of America

⁵ Duke Comprehensive Epilepsy Center, Duke University School of Medicine, Durham, NC, United States of America

* Author to whom any correspondence should be addressed.

E-mail: j.viventi@duke.edu

Keywords: ADC artifacts, electrophysiology, high resolution, neural interfaces, amplifier chips, headstage, Intan Technologies

Supplementary material for this article is available [online](#)

Abstract

Objective. Intan Technologies' integrated circuits (ICs) are valuable tools for neurophysiological data acquisition, providing signal amplification, filtering, and digitization from many channels (up to 64 channels/chip) at high sampling rates (up to 30 kSPS) within a compact package ($\leq 9 \times 7$ mm). However, we found that the analog-to-digital converters (ADCs) in the Intan RHD2000 series ICs can produce artifacts in recorded signals. Here, we examine the effects of these ADC artifacts on neural signal quality and describe a method to detect them in recorded data.

Approach. We identified two types of ADC artifacts produced by Intan ICs: 1) jumps, resulting from missing output codes, and 2) flatlines, resulting from overrepresented output codes. We identified ADC artifacts in neural recordings acquired with Intan RHD2000 ICs and tested the repeated performance of 17 ICs *in vitro*. With the on-chip digital-signal-processing disabled, we detected the ADC artifacts in each test recording by examining the distribution of unfiltered ADC output codes. **Main Results.** We found larger ADC artifacts in recordings using the Intan RHX data acquisition software versions 3.0–3.2, which did not run the necessary ADC calibration command when the inputs to the Intan recording controller were rescanned. This has been corrected in the Intan RHX software version 3.3. We found that the ADC calibration routine significantly reduced, but did not fully eliminate, the occurrence and size of ADC artifacts as compared with recordings acquired when the calibration routine was not run ($p < 0.0001$). When the ADC calibration routine was run, we found that the artifacts produced by each ADC were consistent over time, enabling us to sort ICs by performance. **Significance.** Our findings call attention to the importance of evaluating signal quality when acquiring electrophysiological data using Intan Technologies ICs and offer a method for detecting ADC artifacts in recorded data.

1. Introduction

Intan Technologies' integrated circuits (ICs) are highly valuable tools for acquiring neurophysiological data. Each Intan IC contains miniaturized front-end circuitry for signal amplification, filtering, multiplexing (32:1) and digitization from many channels (up to 64 channels/chip) at high sampling

rates (up to 30 kSPS), all within a single compact package [1]. These features have made Intan ICs widely popular across the neuroscience and neural engineering communities, enabling breakthrough, high-channel-count electrophysiology technologies and neuroscience experiments in freely-moving small animals [2–8], non-human primates (NHP) [9–11], and human subjects [6, 7, 12–14],

which were previously infeasible with large amplifier systems.

While Intan ICs' small chip designs offer significant advantages for neural data acquisition, we found that the miniaturized 16-bit successive approximation register (SAR) analog-to-digital converter (ADC) in the Intan RHD2000 series ICs can produce artifacts in the acquired signals. We found two types of established ADC errors in our testing of the Intan ICs—missing codes (integers) and missing decision levels [15, 16]. The ADC's missing codes result in rapid jumps to incorrect output codes in the signal waveform, which we refer to as jump artifacts, and the ADC's missing decision levels result in strings of incorrectly maintained output codes in the signal waveform, which we refer to as flat-line artifacts. Both artifacts can affect the time series and spectral power of neural recordings. We found that the Intan IC's ADC artifacts are greatly reduced, although not entirely eliminated, by running the ADC calibration routine specified in the Intan RHD2000 datasheet [1]. However, Intan RHX data acquisition software versions 3.0–3.2 did not include the ADC calibration routine when recording controller inputs were rescanned, resulting in potentially more significant artifacts in data collected with these software releases. The updated Intan RHX software version 3.3 includes the recalibration routine in the rescan function, which we found greatly reduced the occurrence and size of ADC artifacts. Here, we report on our characterization of these ADC artifacts, their effects on neural signal quality, methods for detecting ADC artifacts in recorded data, and an approach for choosing the best performing Intan ICs.

2. Methods

2.1. *In vitro* recordings with intan RHD2000 ICs

We recorded test signals in saline using custom liquid crystal polymer thin-film (LCP-TF) micro-electrocorticographic (μ ECoG) arrays connected to custom connector boards and either custom headstages or headstages acquired directly from Intan Technologies (#C3315 RHD 64-ch and #C3314 RHD 32-ch) (figure 1). Each headstage, custom or acquired directly from Intan Technologies, included one RHD2000 series IC with 32 (RHD2132) or 64 (RHD2164) recording channels. Each RHD2000 series IC has one ADC per 32 channels. For recordings from custom headstages, we used micro-high-definition multimedia interface (μ HDMI) cables connected to serial peripheral interface (SPI) cables to carry digital signals from the headstage to the Intan Recording Controller or Open Ephys Acquisition Board. Only SPI cables were used directly for recordings from Intan Technologies headstages acquired directly from Intan (not custom).

The Intan Recording Controller was operated using Intan Technologies RHX Software (versions 3.0–3.3) and the Open Ephys Acquisition Board was operated using the Open Ephys GUI v0.6.6. All recordings were collected at a sampling rate of 20 kSPS with on-chip digital signal processing (DSP) disabled and the amplifier bandwidth programmed to 0.1 Hz–10 kHz. Further details on the LCP arrays and custom headstages can be found in Chiang *et al* [7].

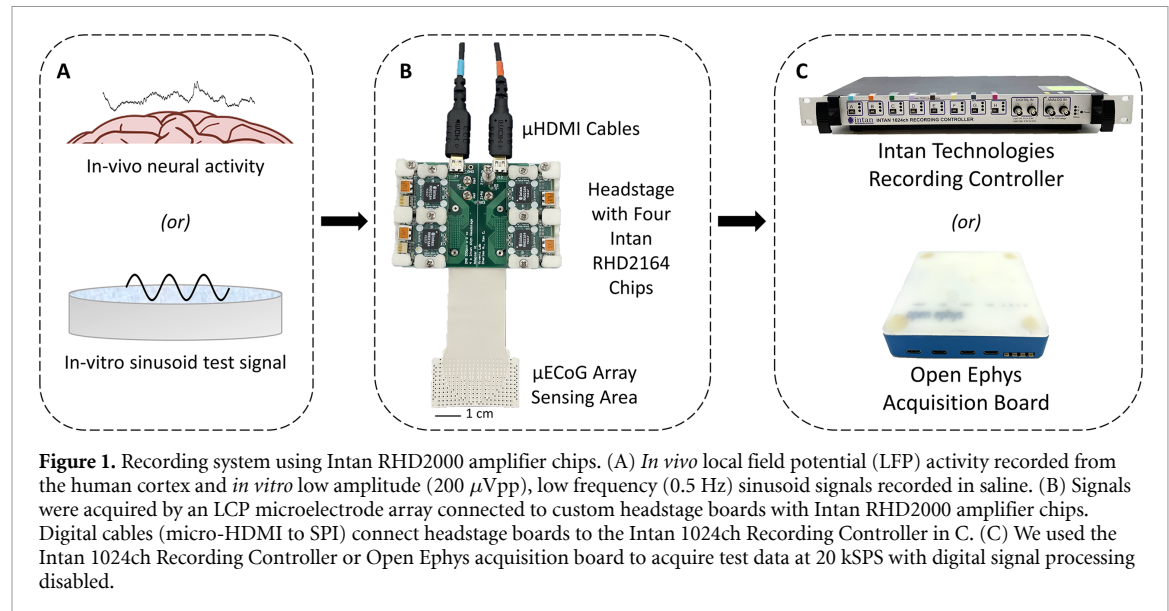
We characterized ADC performance on RHD2164 chips by applying sinusoidal (200μ Vpp, 0.5 Hz) test signals produced by a Wavetek Model 25 Precision 5 MHz function generator connected to a gold wire near an LCP-TF μ ECoG array in saline. We compared artifacts produced by uncalibrated and calibrated ADCs using Intan RHX software version 3.2 and Intan RHX software version 3.3, respectively. The Intan RHD2132 headstage provides access to an auxiliary channel which is directly connected to the multiplexer and ADC, bypassing the chip's amplifier channels (supplemental figure 1). We used this RHD2132 headstage to test the Intan ADC across the full voltage range at the auxiliary inputs (0.1 V–2.45 V) using a low frequency, high amplitude triangular waveform (2.8 Vpp, 1.2 V offset, 0.1 Hz) (supplemental figures 1 and 2).

2.2. Intraoperative recordings with intan RHD2000 ICs

In previous studies we, used our LCP-TF μ ECoG arrays with custom Intan RHD2164 headstages (figure 1) to record intraoperatively from the cortex of patients undergoing neurosurgery for the treatment of epilepsy or implantation of a deep brain stimulator [7, 12, 13, 17]. We used μ HDMI cables connected to SPI cables to carry digital signals from the headstages within the operating room sterile zone to the Intan recording controller outside of the sterile zone. All intraoperative neural recordings presented in this paper were collected using Intan RHX software version 3.2 to interface with the Intan recording controller. Recordings were collected at a sampling rate of 20 kSPS with the amplifier bandwidth set to 0.1 Hz–10 kHz.

2.3. Analysis of intraoperative neural recordings

We evaluated the effects of ADC artifacts on the spectral content of neural time series and the detectability of neural signals of interest gathered during intraoperative recordings. All signal processing was conducted using custom or previously published MATLAB code (MathWorks Inc., Natick, MA). We examined the neural time series before down-sampling or digital filtering was applied to clearly visualize the ADC artifacts (figures 2(A) and (B-i)). We then decimated the data to 2 kSPS (Chebyshev Type I



infinite impulse response filter of order 8) (figure 2(B-ii)). We band-pass filtered (Chebyshev Type II infinite impulse response filter, applied forward and reverse) the decimated data in the 80–500 Hz band (figure 2(B-iii)) to look for the presence of high-frequency oscillations (HFOs), a biomarker of epileptic tissue [18]. We implemented a commonly used HFO detection algorithm developed by Staba *et al* using a previously published open-source software (RippleLab version 3, accessed July 2020 (<https://github.com/BSP-Uniandes/RIPPLELAB/>) to detect HFOs in the bandpass filtered signal [18, 19]. We additionally high-pass filtered (Chebyshev Type II infinite impulse response filter, applied forward and reverse) the 20 kSPS signal to >300 Hz (figure 2(B-iv)) to assess the effect of the digital artifacts in the neural spiking band. We used a normalized Morse wavelet transform to create time-frequency plots of the unfiltered, full sampling rate (20 kSPS) neural time series (figure 2(B-v)) to visualize the effect of the ADC artifacts on spectral power.

2.4. Identifying ADC artifacts

We modified the MATLAB RHD file reader code (www.intantech.com, February 8 2021) to save the time series ADC integer values rather than the voltage values so that the ADC output could be evaluated directly. For recordings collected with the on-chip DSP option disabled, we created histograms of each channel's ADC integers with a bin-width of one (figures 3 and 4). We identified missing integer values with no occurrences within the signal range of the histogram. Consecutive integers with no occurrence in the histogram reflect the size of the digital jump artifacts seen in the time series. We also identified integer values that had abnormally high occurrences. These over-represented integer values correspond to

the flat-line artifacts in the time series. All histograms were generated from the full sampling rate data (20 kSPS).

2.5. Characterizing ADC performance

We measured the maximum jump artifact size in 2 min sinusoidal test recordings as described in methods section 2.1 from 34 ADCs on 17 Intan RHD2164 ICs. Each IC included two ADCs (A,B). ICs 1–16 were on custom headstage boards while IC 17 was on a headstage board acquired directly from Intan Technologies. We tested each ADC 10 times in the uncalibrated and calibrated states. Between each test, we power-cycled the chip by unplugging and re-plugging the SPI cable and rescanned the recording controller inputs. We acquired uncalibrated recordings by rescanning the recording controller inputs in RHX software version 3.2 before recording data and acquired calibrated recordings by rescanning the recording controller inputs in RHX software version 3.3 before recording data.

We characterized the size of digital jump artifacts using the histogram of ADC outputs. We evaluated the histogram of each channel's ADC output only within the range of the recorded signal amplitude ($200 \mu\text{Vpp}$) centered around the mean. This avoided falsely counting un-sampled integer values at the edges of the distribution. For a given recording, we summed the histograms across all 32 channels corresponding to each ADC on the Intan IC, creating a single histogram for each ADC (supplemental figure 3). We excluded high-impedance ($>100 \text{ k}\Omega$ tested at 1 kHz) or open channels from analysis. For each ADC histogram, we identified the maximum jump artifact size as the length of the longest string of consecutive integers with zero occurrence.

2.6. Statistical analysis

We used a two-tailed t-test to compare the maximum jump artifact size measured across all ADCs in the calibrated test recordings with those in the uncalibrated test recordings. We used a one-way ANOVA to compare the distributions of the maximum jump artifact size between all 34 ADCs in the calibrated state.

3. Results

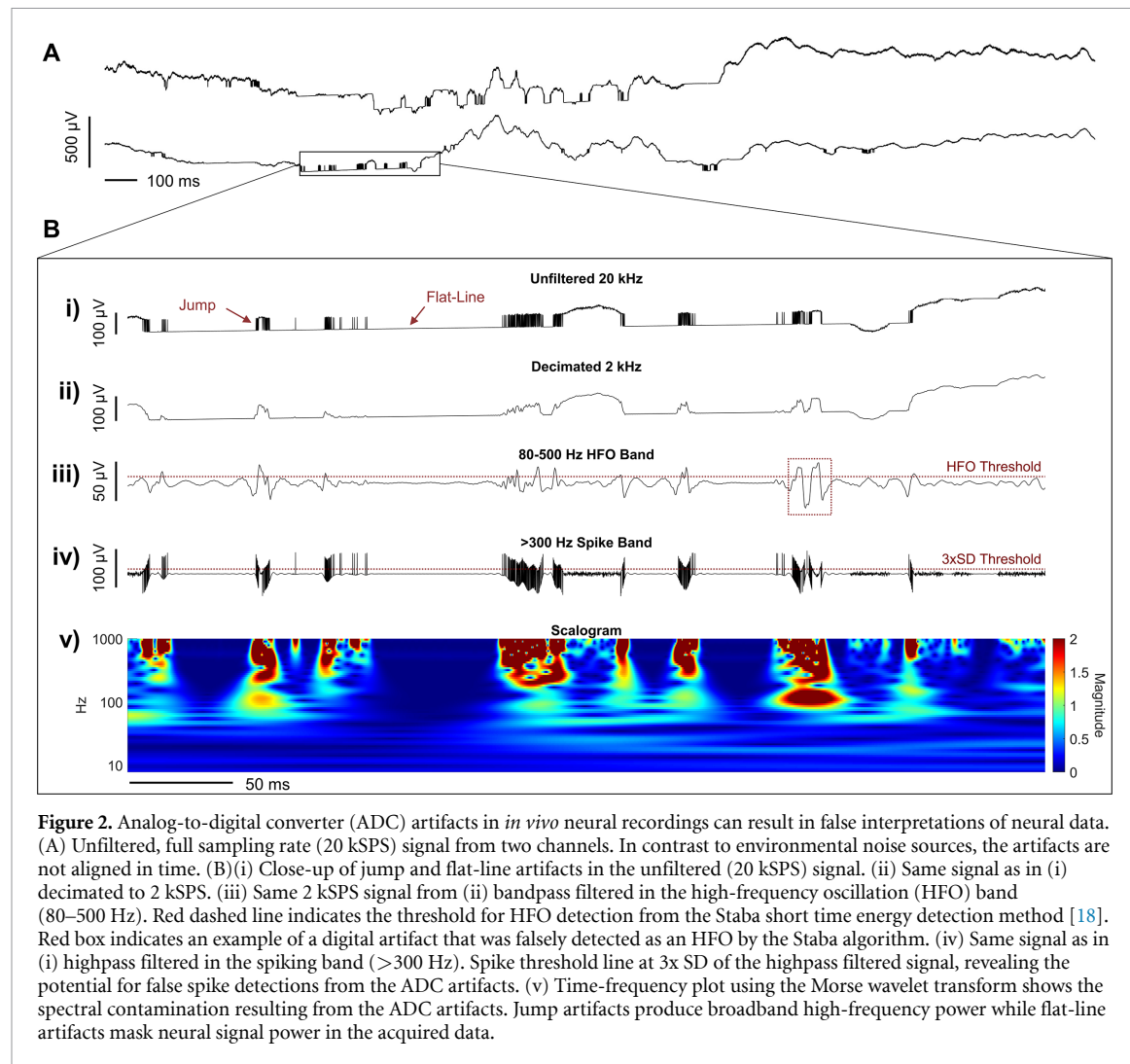
We visually identified jump and flat-line ADC artifacts in an intraoperative neural recording from the cortex of a patient undergoing surgery for the treatment of epilepsy (figure 2). We found that these artifacts are most distinctly visible in the unfiltered, full sampling rate data (20 kSPS) (figure 2(B-i)). The scalogram reveals that the sharp jump artifacts have broadband power in the higher frequency ranges and the flat-line artifacts mask the underlying neural activity (figure 2(B-v)). When filtered in frequency ranges of interest, the high-frequency power of the jump artifacts complicated detection of neural signals. In this neural recording, we were interested in capturing HFOs, an interictal biomarker of epileptic tissue [17]. When filtered in the HFO band (80–500 Hz), we found that the jump artifacts produced oscillations which resembled HFOs and were falsely identified by the first thresholding stages of an automated detection process (figure 2(B-iii)) [18]. We later discarded this false detection using an artifact rejection method which applies a threshold to the derivative of the signal [17]. In addition, the jump artifacts exceeded a basic spike detection threshold of 3x the SD of the signal in the >300Hz frequency range, potentially complicating neural spike detection in the data (figure 2(B-iv)).

We found that turning off the on-chip DSP on the Intan ICs enabled clearer visualization of the ADC artifacts. In *in vitro* sinusoid testing and *in vivo* neural recordings using Intan RHX Software v3.2, we found that jump and flat-line artifacts occurred at consistent voltage levels within a recording (figure 3). These voltage levels correspond to integer powers of two in the ADC output code (figure 3). In the histogram of ADC integers, we observed the jump artifacts as ranges of integers that were consistently unsampled and the flat-line artifacts as particular integers that were over sampled by the ADC (figure 3(B) and (D)). Using the auxiliary input to the RHD2132 headstage, we were able to bypass the amplifier stage and directly test the Intan IC's ADC using a triangular waveform and found that the ADC artifacts can occur across the full range of ADC integers (supplemental figure 1). This is also seen in the histogram of ADC integers, showing missing and overrepresented output codes (supplemental figure 1). We also found that the size and location of the artifacts within the

ADC integer range was consistent across all 32 channels that share the same ADC (supplemental figure 4). The manifestation of these incorrect output code assignments can be seen in the bit code readout of the jump and flat-line artifacts (supplemental figure 5).

Upon further testing, investigation into the Intan RHX software, and discussion with Intan Technologies, we found that the requisite ADC calibration routine specified in the RHD2000 IC datasheet was only run at software startup in versions 3.0–3.2 [1]. If additional headstages were connected to the Intan RHD recording controller and the software's headstage rescan function was used, then the ADC calibration routine was not run, and recordings were collected with uncalibrated ADCs (figure 3). This was corrected in an updated version of Intan RHX Software v3.3. We found that recordings collected with correctly calibrated ADCs using this updated software had greatly reduced ADC artifacts (figures 4 and 5). Some *in vitro* sinusoid recordings and *in vivo* neural recordings collected with on-chip DSP disabled and the ADC calibration routine run were free of jump or flat-line artifacts, confirmed by visualization of the time series and a histogram of ADC integers with no gaps or peaks (figures 4 (A)–(D)). A triangle wave recording using a calibrated 32-channel ADC did not show evidence of artifacts across the full integer range (supplemental figure 2). However, we found that the ADC calibration routine did not fully prevent ADC artifacts, with some calibrated recordings still showing artifacts (figures 4(E) and (F)). With repeated testing of 17 Intan RHD ICs, we found that the ADC calibration routine did not fully eliminate but significantly reduced the occurrence and size of ADC artifacts (figure 5). The mean size of jump artifacts measured in uncalibrated recordings ($7.1 \pm 9.1 \mu\text{Vpp}$, $n = 340$) was significantly greater ($p < 0.0001$) than the mean size of jump artifacts in calibrated recordings ($0.79 \pm 1.2 \mu\text{Vpp}$, $n = 340$) (figure 5(B)).

In addition, calibrated ADCs had more consistent jump artifact size between repeated measurements (figure 5). Specifically, the variance in artifact size between calibrated ADCs was greater than the variance in artifact size between repeated tests of the same ADC (ANOVA, $p < 0.0001$), indicating that individual ADCs may be separable by performance (figure 5(A)). We found that when calibrated, 25/34 (73.5 %) ADCs had jump artifacts with a mean size $\leq 1.8 \mu\text{Vpp}$ and 9/34 (26.5%) had jump artifacts with a mean size $> 1.8 \mu\text{Vpp}$ (figure 5(A)). We found that calibrated ADC artifact size remained consistent over multiple days of testing, and that ADCs with small, medium, and large jump artifacts were clearly separable from one another (figure 6(A)). We also found that the ADC performance when using the Open Ephys acquisition system closely matched that



of the Intan Technologies recording controller and RHX software v3.3 (figure 6(B)). This result additionally confirmed that the Open Ephys GUI v0.6.6 correctly runs the ADC calibration routine.

4. Discussion

Through our testing of Intan RHD2000 ICs, we found that their ADCs can produce artifacts due to missing or overrepresented ADC output codes. These ADC artifacts affect the detectability of neural signals of interest and alter the spectral content of the neural data by adding noise to the recorded time series (figure 2). Histograms of the ADC integers provide a useful tool for identifying missing and overrepresented ADC output codes corresponding to jump and flat-line artifacts, respectively (figures 3 and 4). The size of ADC jump artifacts is significantly reduced by the ADC calibration routine specified in the Intan RHD2000 datasheet (figures 4 and 5). However, this calibration routine was missing from the port rescan operation in the Intan RHX software versions 3.0–3.2 (figures 3 and 5). When using these software versions,

rescanning the inputs to the Intan recording controller significantly increased the size of jump artifacts in the recorded signal because the ADCs were not calibrated (figure 5). Data collected without use of the rescan function in the Intan RHX software versions 3.0–3.2 correctly ran the calibration routine and therefore resulted in smaller ADC artifacts. This software bug has been corrected in Intan RHX software version 3.3 so that ADC calibration is run during the software start up and during the port rescan operation (figures 4 and 5). Based on review of our own prior data, we also believe, but have not confirmed, that the older Intan RHD data acquisition software prior to RHX v3.0 correctly ran the ADC calibration routine. The size of jump artifacts in data collected with the Open Ephys acquisition board and GUI version 0.6.6 closely match the small jump artifacts observed when using Intan RHX software version 3.3 with the calibration routine (figure 6(B)). This indicates that when calibrated, the variation in artifact is dependent on the Intan IC's ADC, not the acquisition system used. This also provides evidence that the Open Ephys GUI v0.6.6 correctly runs the ADC calibration routine.

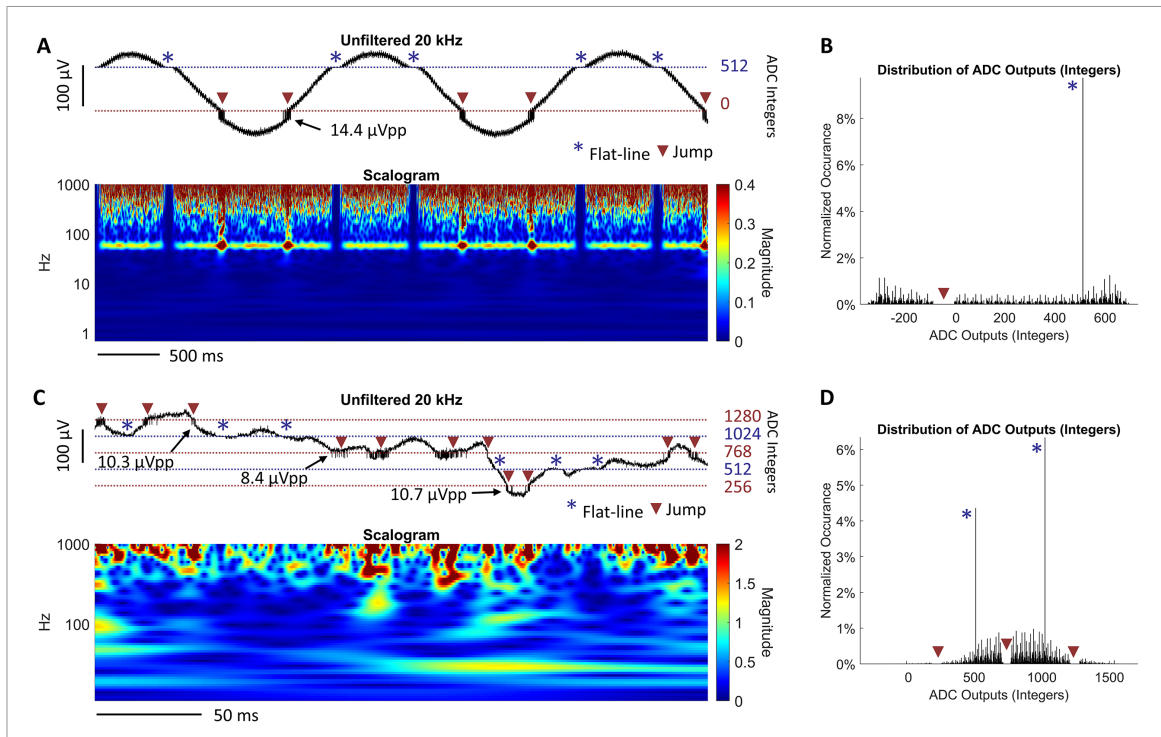


Figure 3. Digital artifacts are prominent when the analog-to-digital converter (ADC) is uncalibrated. (A) Unfiltered, full sampling rate (20 kSPS) recording of a sinusoidal test signal (0.5 Hz, 200 μ Vpp) with digital signal processing (DSP) disabled and no ADC calibration routine. Red triangles mark the jump artifacts (14.4 μ Vpp) and blue asterisks mark the flat-line artifacts observed in the time series (top) and scalogram (bottom). (B) Histogram of the ADC integers sampled over 1 min in the recording shown in (A). The red triangle marks the jump artifact seen as a gap of missing integers, and the blue asterisk marks the flat-line artifacts seen as a peak of overrepresented integers in the histogram. (C) Unfiltered (20 kSPS) signal from an intraoperative neural recording collected with DSP disabled and no ADC calibration routine. Red triangles mark the jump artifacts (10.7 μ Vpp) and blue asterisks mark the flat-line artifacts observed in the time series (top) and scalogram (bottom). (D) Histogram of all ADC integers sampled over 1 min of the recording shown in (C). The red triangles mark the jump artifacts seen as gaps of missing integers, and the blue asterisks mark the flat-line artifacts seen as peaks of overrepresented integers in the histogram.

When calibrated, we found that the size of jump artifacts was reduced ($<5 \mu$ Vpp) and was highly consistent within a given ADC, even over multiple days of testing (figures 5 and 6). More specifically, the variance in performance between ADCs was greater than the variance in performance between repeated tests of the same ADC (ANOVA, $p < 0.0001$). This enabled us to reliably differentiate between better and worse performing ADCs (figures 5 and 6). We found jump artifacts $\leq 1.8 \mu$ Vpp to be acceptable for our neural recordings of LFP from the cortical surface, and therefore chose ICs based on this threshold. However, others may have a different noise requirement depending on their frequency range of interest or overall system noise and therefore may choose a different threshold by which to screen the performance of their Intan ICs. We have provided example test signals with a range of jump artifact sizes for readers to determine their own artifact tolerance (supplemental figure 6). We have focused on quantification of jump artifacts in our testing of ADCs. This is motivated by the fact that jump artifacts could contribute to false detection of neural signals of interest due to their power in high frequency ranges (figure 2). In contrast, flat-line artifacts result in a loss of signal power due to masking of underlying neural activity, but do not produce false signal power in frequency ranges of interest (figure 2).

However, the importance of flat-line artifacts depends on the particulars of each user's experiment (figure 2).

Despite the complication these artifacts pose to accurate neural signal acquisition, Intan Technologies' ICs still provide a very powerful tool for high-channel count electrophysiology. The ADC artifacts we have found are not unique to the ADCs used in the Intan ICs and are routinely characterized in industry-standard ADC testing [15, 16]. The imperfections of the Intan ICs' ADCs likely reflect a design trade-off between performance and the components' compact footprints—an essential feature of the Intan ICs, particularly in the case of freely moving experiments where large amplifier chips would preclude high-channel count recordings. We have not identified a compelling alternative to the Intan ICs for our experimental needs and find that when the ADCs are correctly calibrated, many have acceptable artifact sizes (figure 5, supplemental figure 6).

However, from these results, we have several recommendations for readers to consider when using Intan ICs. We recommend that all users of the Intan RHX software update to version 3.3.0 or later to ensure that the ADCs are being recalibrated when the rescan function is used. We also recommend disabling the on-chip DSP through the Intan RHX software or Open Ephys GUI. If DSP is enabled, then the data is

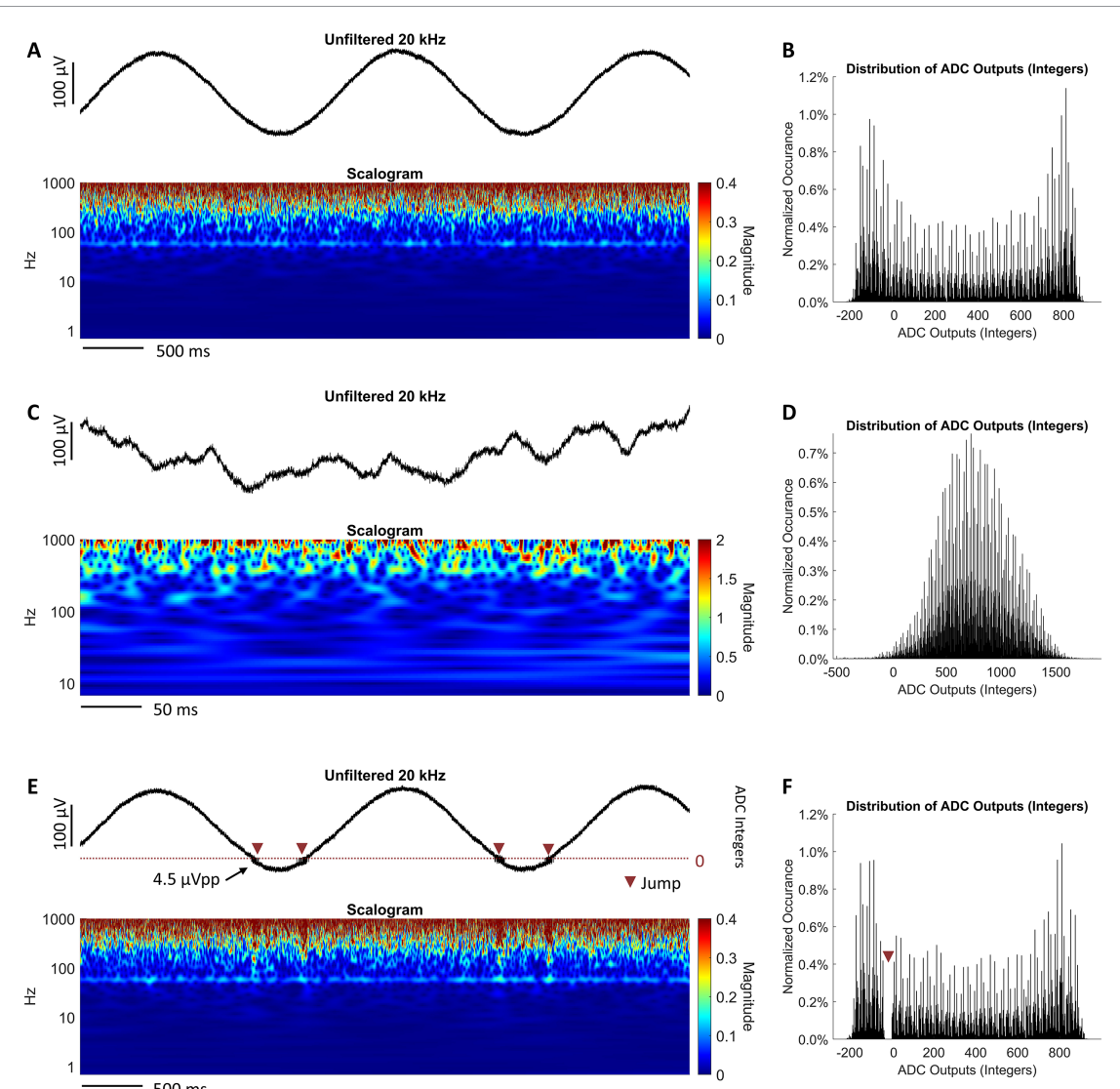


Figure 4. Software ADC calibration routine reduces the size of the ADC artifacts. (A) Unfiltered, full sampling rate (20 kSPS) recording of a sinusoidal test signal (0.5 Hz, 200 μ Vpp) with DSP disabled and the ADC calibration routine run. No jump or flat-line artifacts were visible in the time series (top) or scalogram (bottom). (B) Histogram of the ADC integers sampled over 1 min during the sinusoidal recording shown in (A) with no missing or overrepresented integers. (C) Unfiltered (20 kSPS) signal from an intraoperative recording collected with DSP disabled and the ADC calibration routine run. No jump or flat-line artifacts were visible in the time series (top) or scalogram (bottom). (D) Histogram of the ADC integers sampled over 1 min in the recording shown in (C) with no missing or overrepresented integers. (E) Unfiltered (20 kSPS) recording of a sinusoidal test signal (0.5 Hz, 200 μ Vpp) with DSP disabled and the ADC calibration routine run. Red triangles mark the jump artifacts (4.5 μ Vpp) which were still observed after calibration in the time series (top) and scalogram (bottom). (F) Histogram of the ADC integers sampled over 1 min in the recording shown in (E). Red triangle marks the jump artifacts seen as a gap in the histogram of ADC integers.

filtered before it is saved, precluding generation of a histogram of raw ADC integers which provides the simplest method for detection of the ADC artifacts. However, if previous data has been collected with the on-chip DSP enabled, then the presence of ADC artifacts may be found by close examination of the time series at the original sampling rate and without any additional filtering in software. Down sampling or filtering the data distorts the ADC artifacts, making them less clearly identifiable (figure 2). Additionally, if the rescan function was not used during previous

data collection, then the ADCs should have been correctly calibrated in recordings with Intan RHX software v3.0–3.2. We also encourage users to screen their Intan ICs for better and worse performing ADCs. Each user's threshold for acceptable artifact size may differ depending on the electrophysiological activity of interest (supplemental figure 6). It should also be noted that we have not tested Intan Technologies' RHS ICs for ADC artifacts and would encourage users of those ICs to replicate these testing methods to screen for ADC artifacts.

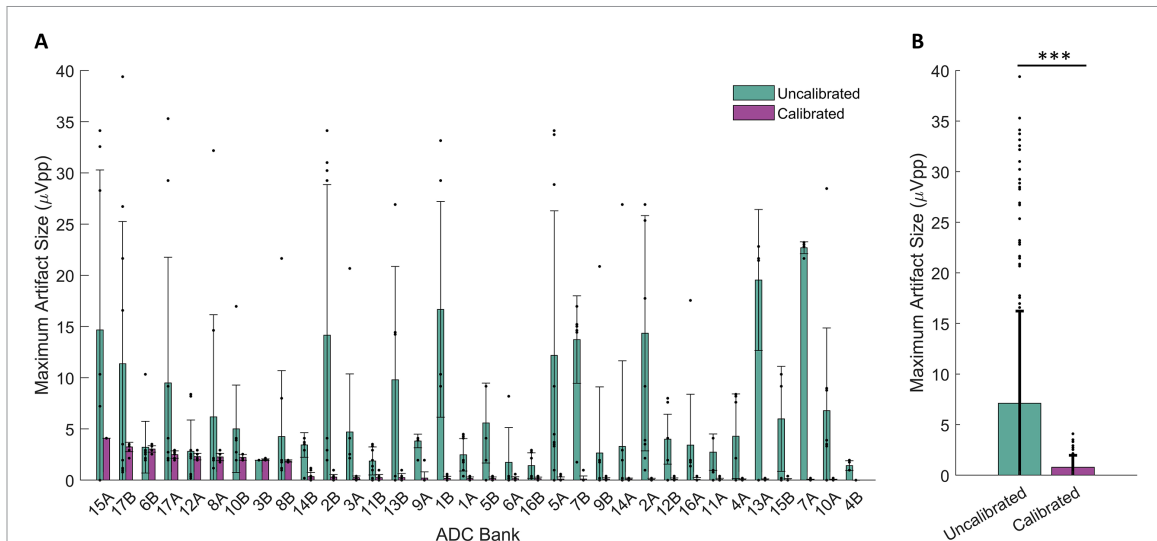


Figure 5. ADC calibration reduces, but does not always eliminate, the jump artifacts in repeated *in vitro* recordings of Intan RHD2000 ICs. (A) Maximum jump artifact size measured for each ADC (A&B) from 17 ICs. ICs 1–16 were mounted on custom headstage boards (figure 1) while IC 17 was on an Intan 64-Channel Headstage board (Part #C3315). We tested each IC 10 times without ADC calibration (blue) and with ADC calibration (orange) using a sinusoidal test signal (0.5 Hz, 200 μVpp) in saline. Each data point represents one test and each bar shows the mean and standard deviation across tests for each ADC. For all ADCs, the calibration routine reduced the mean maximum size of the jump artifacts. When calibrated, 25/34 (73.5%) ADCs had jump artifacts $\leq 1.8 \mu\text{Vpp}$ and 9/34 (26.5%) had jump artifacts $> 1.8 \mu\text{Vpp}$. Bars are sorted from left to right by the mean maximum artifact size after calibration. In calibrated recordings, the variance in performance between ADCs was greater than the variance in performance between repeated tests of the same ADC (ANOVA, $p < 0.0001$). (B) Bars show the mean maximum artifact size between all uncalibrated ($n = 340$) and calibrated ($n = 340$) ADC tests. The error bars show the standard deviation across tests. Calibrated ADCs performed significantly better than uncalibrated ADCs ($p < 0.0001$).

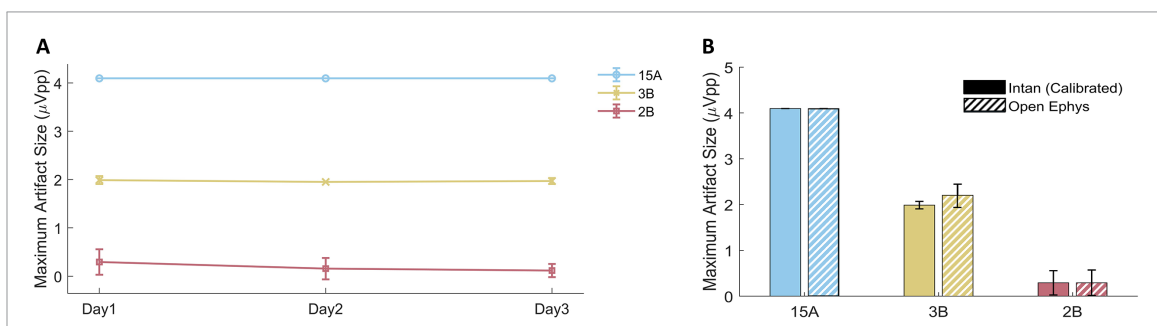


Figure 6. Calibrated ADC performance is consistent across time and across data acquisition systems. (A) Maximum artifact size measured across three days from three calibrated ADCs. Each datapoint shows the mean of the maximum artifact size and the error bars show the standard deviation across 10 tests. Each ADC's performance remained consistent between tests and across multiple days of testing, enabling consistent differentiation between ADCs with small (2B), medium (3B) and large (15 A) artifacts. (B) Maximum artifact size measured from three ADCs using the Intan system (recording controller and Intan RHX software v3.3 including the ADC calibration routine) and the Open Ephys system (Open Ephys acquisition board and software v0.6.6). Each bar shows the mean of the maximum artifact size and the error bars show the standard deviation across 10 tests. ADC 15 A had zero variability in artifact size.

There may be interest in methods to correct the artifacts in previously recorded data, particularly if collected after port rescanning using Intan RHX software versions 3.0–3.2. Because the artifacts occur at consistent levels in the ADC output range but not at consistent time points across channels (supplemental figure 4), noise reduction methods such as common average referencing will not be effective for removing or reducing these artifacts. We have taken the approach of pre-screening our Intan ICs for artifact size rather than attempting to correct the data after recording. However, readers could

explore methods to compress the data at jump artifacts to maintain a more continuous time series (supplemental figure 7). A proof-of-concept of this method is shown in supplemental figure 7, but for the purposes of this publication this method was not fully developed. The specific correction algorithm will vary depending on the pattern of missing output codes and decision levels for each ADC. In the case of flat-line artifacts, we do not envision any obvious method to access the neural signal which was masked by the missing ADC decision levels.

5. Conclusion

Intan Technologies' RHD2000 ICs are valuable tools for recording neurological data, particularly from high-channel count arrays in freely moving animals or spatially constrained experimental settings such as the operating room. However, the ADCs used on the Intan ICs can produce artifacts in the recorded time series due to missing codes (jumps) or missing decision levels (flat-lines) which negatively affect the acquisition of neural signals of interest. We found that Intan RHX software versions 3.0-3.2 exacerbated this problem by failing to run the ADC calibration routine, specified in the Intan Technologies RHD2000 datasheet, when headstage inputs to the recording controller were rescanned. However, when using updated software which correctly performed the ADC calibration, we found that the size of ADC jump artifacts was significantly reduced and, although varying between ADCs, remained highly consistent over time within each ADC. To minimize the size of ADC artifacts from the Intan ICs, we found it essential to use software which correctly performs the ADC calibration routine and to preselect Intan ICs with lower ADC artifacts.

Ethics Statement

The collection of human data included in this article was approved by Duke University Health System Institutional Review Board. This study was performed in accordance with the Nuremberg Code. All adult participants provided written informed consent to participate in this study.

Data availability statement

The data that support the findings of this study are available upon reasonable request from the authors.

Acknowledgments

J.V. receives support from the Department of Defense (EP200077), the National Institutes of Health (U01 NS099697, UG3 NS120172, U01 NS123668, R01 DC019498, Clinical and Translational Science Awards grant UL 1TR002553), and the National Science Foundation (CBET-1752 274). C.S. receives support from the National Science Foundation (Graduate Research Fellowship Program DGE-2139754).

Conflict of interest

Parts of the technology described here are patent pending under 'Electroencephalography (EEG) Electrode Arrays and Related Methods of Use' U.S. Patent Application # PCT/US2020/051400. The authors have no further conflicts of interest to disclose.

ORCID iDs

- Katrina Barth <https://orcid.org/0000-0002-0193-5057>
Cecilia Schmitz <https://orcid.org/0009-0003-7918-3080>
Thomas Jochum <https://orcid.org/0000-0001-6155-3088>
Jonathan Viventi <https://orcid.org/0000-0001-6054-0541>

References

- [1] Intan Technologies, LLC 2023 *RHD2000 Series Digital Electrophysiology Interface Chips*
- [2] Guitchounts G, Markowitz J E, Liberti W A and Gardner T J 2013 A carbon-fiber electrode array for long-term neural recording *J. Neural Eng.* **10** 046016
- [3] Schneider D M, Nelson A and Mooney R 2014 A synaptic and circuit basis for corollary discharge in the auditory cortex *Nature* **513** 189–94
- [4] Wu F *et al* 2015 Monolithically integrated μ LEDs on silicon neural probes for high-resolution optogenetic studies in behaving animals *Neuron* **88** 1136–48
- [5] Geiller T, Fattah M, Choi J-S and Royer S 2017 Place cells are more strongly tied to landmarks in deep than in superficial CA1 *Nat. Commun.* **8** 14531
- [6] Khodagholy D *et al* 2015 NeuroGrid: recording action potentials from the surface of the brain *Nat. Neurosci.* **18** 310–5
- [7] Chiang C H *et al* 2021 Flexible, high-resolution thin-film electrodes for human and animal neural research *J. Neural Eng.* **18** 045009
- [8] Woods V *et al* 2018 Long-term recording reliability of liquid crystal polymer microECoG arrays *J. Neural Eng.* **15** 066024
- [9] Schwarz D A *et al* 2014 Chronic, wireless recordings of large-scale brain activity in freely moving rhesus monkeys *Nat. Methods* **11** 670–6
- [10] Zaaimi B *et al* 2022 Closed-loop optogenetic control of the dynamics of neural activity in non-human primates *Nat. Biomed. Eng.* **7** 559–75
- [11] Kaiju T, Inoue M, Hirata M and Suzuki T 2021 High-density mapping of primate digit representations with a 1152-channel microECoG array *J. Neural Eng.* **18** 036025
- [12] Sun J *et al* 2022 Intraoperative microseizure detection using a high-density micro-electrocorticography electrode array *Brain Commun.* **4** fcac122
- [13] Duraivel S *et al* 2023 High-resolution neural recordings improve the accuracy of speech decoding *Nat. Commun.* **14** 6938
- [14] Yang J C *et al* 2021 Microscale dynamics of electrophysiological markers of epilepsy *Clin. Neurophysiol.* **132** 2916–31
- [15] Burns M R and Gordon W 2001 *An Introduction to Mixed-Signal IC Test and Measurement* (Oxford University Press)
- [16] Huang J L, Huang X L, Chou Y F and Kwai D M 2012 A SAR ADC missing-decision level detection and removal technique *2012 IEEE 30th VLSI Test Symp. (VTS)* (23–25 April 2012)
- [17] Barth K J *et al* 2023 Flexible, high-resolution cortical arrays with large coverage capture microscale high-frequency oscillations in patients with epilepsy *Epilepsia* **64** 1910–24
- [18] Staba R J, Wilson C L, Bragin A, Fried I and Engel J 2002 Quantitative analysis of high-frequency oscillations (80–500 Hz) recorded in human epileptic hippocampus and entorhinal cortex *J. Neurophysiol.* **88** 1743–52
- [19] Navarrete M, Alvarado-Rojas C, Le Van Quyen M and Valderrama M 2016 RIPPLELAB: a comprehensive application for the detection, analysis and classification of high frequency oscillations in electroencephalographic signals *PLoS One* **11** e0158276